Extreme ultraviolet light source development to enable pre-production mask inspection

Matthew J. Partlow*, Matthew M. Besen, Paul A. Blackborow, Ron Collins, Deborah Gustafson,

Stephen F. Horne, Donald K. Smith

Energetiq Technology, Inc., 7 Constitution Way, Woburn, MA, USA 01801

ABSTRACT

As extreme ultraviolet (EUV) lithography moves into pre-production, the requirement for commercially available mask metrology tools becomes more urgent. A key to developing a successful tool is a reliable high brightness EUV light source. The Energetiq EQ-10 is a commercially available EUV light source, with an installed base of over 15 sources in the field. The source relies on an electrodeless Z-pinch™ to produce greater than 10 Watts/2π of 13.5 nm 2% bandwidth (BW) light. In order to meet brightness and stability requirements of mask metrology tools, we have investigated modifications to the original design of the EQ-10. The result of these modifications has roughly doubled the source output power, and has achieved brightness greater than 8 Watts/mm^2/sr, without sacrificing the spatial and pulse-to-pulse stability of the original design. This level of performance is sufficient for initial mask blank and imaging inspection tools.

Keywords: Z-pinch, electrodeless, extreme ultraviolet, mask metrology, mask inspection, discharge produced plasma

* mpartlow@energetiq.com; phone: 1-781-939-0763; fax: 1-781-939-0769; http://www.energetiq.com

1. INTRODUCTION

The lack of mask inspection tools for EUV lithography has been identified as a remaining stumbling block that threatens the future of EUV amongst the competing technologies. Key characteristics of a successful metrology light source include high brightness, excellent spatial stability, good pulse-to-pulse stability, clean photons, and high overall system reliability. The EQ-10 [1] is already a highly reliable system with proven spatial and pulse stability. It is currently being used as a light source for laboratory based actinic full-field mask blank inspection [2][3][4]. Requirements have been identified by the major tool inspection and metrology manufacturers outlining brightness needs to ensure a high throughput, high sensitivity tool required by the fabs. Source brightness on the order of 10 Watts/mm^2/sr is considered sufficient for initial actinic aerial imaging mask inspection tools at the 16 nm hp node [5]. By enhancing the performance of Energetiq's standard EQ-10 source, that brightness level has been substantially achieved. Further enhancements will be needed for subsequent generations.

In this paper we first review key components and operating principles of the EQ-10 electrodeless Z-pinch light source. We then describe the recent design modifications, which include increased system power handling and electrical pulse reproducibility, and report on the impact of this redesign on source performance. Last, we discuss the potential for scaling the EQ-10 light source to higher brightness.

2. ELECTRODELESS Z-PINCH SOURCE CONCEPT

The so-called Z-pinch is a well known method for creating hot plasmas to produce energetic photons [6][7]. The unique design of the EQ-10 discharge plasma Z-pinch source relies on induction via a

transformer core to generate the Z-pinch current, whereas traditional Z-pinch sources rely on conduction via electrodes. In the basic concept, the transformer primary circuit consists of two copper plates, electrically connected at their centers by a conductive tube or bore. The primary current flows radially in on one plate, axially through the central connection, and radially outward through the second plate. This structure is shown in cross-section in Figure 1(b). The induced secondary currents flow in a Xenon plasma through three electrically parallel paths which pierce the primary structure in three places, and then combine in the central bore (plasma loops are shown in blue in Figure 1(c)). The structure is surrounded by a vacuum vessel, in which a xenon pressure in the 100 millitorr range in maintained.

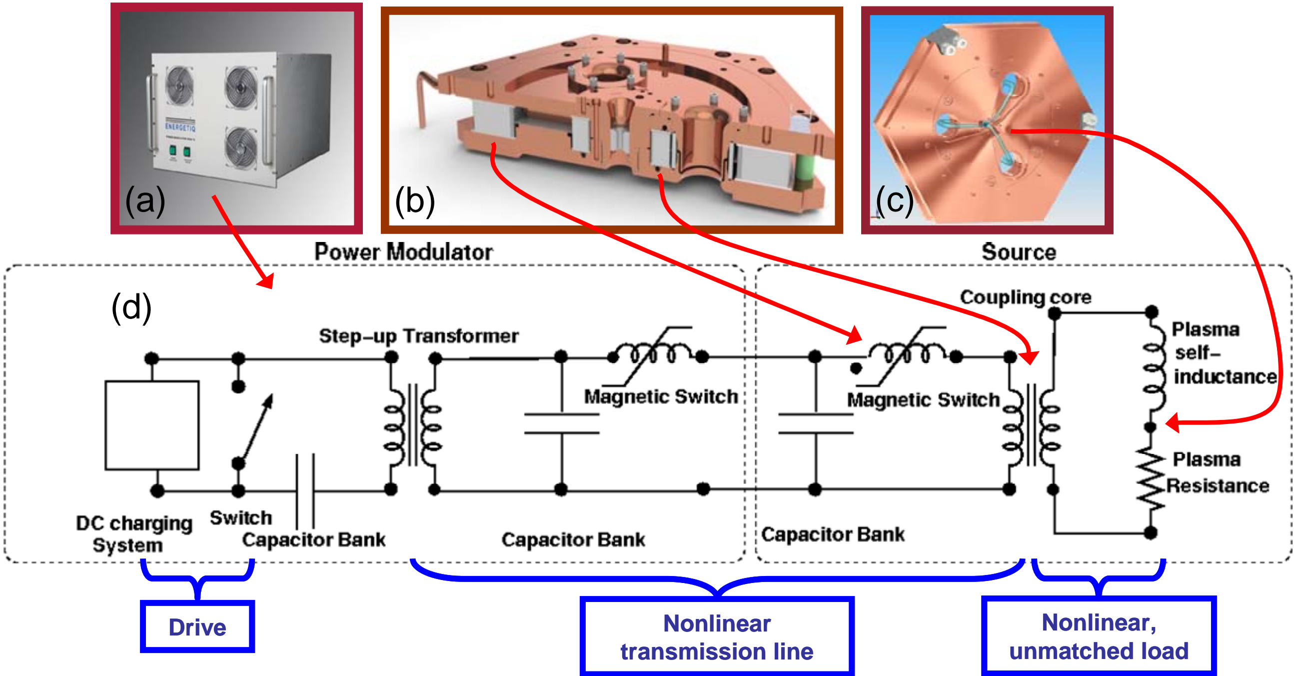

Figure 1. Illustrations (a-c) and schematic (d) demonstrating the key structures of the Xenon electrodeless Z-pinch EUV light source.

Sandwiched between the plates are two magnetic cores (non-central grey structures in Figure 1(b)). The inner core, closely surrounding the central bore, provides the magnetic flux linkage between the primary current path through the copper, and the three parallel secondary currents flowing in the plasma (which combine in the bore to generate the magnetic Z-pinch). The second core is near the outer radius of the device, and surrounds the three plasma return holes. This saturable core functions as a magnetic switch / current pulse compressor with a specific volt-second capacity.

In operation, a capacitor bank (shown schematically in the "Source" section of Figure 1(d)) is connected across the copper plates – symmetrically, with connections to each of the six facets of the copper plates. A pulse forming system, termed the modulator (as shown in Figure 1(a) and schematically in the "Power Modulator" section of Figure 1(d)) generates a fast electrical pulse that is applied to the plates, causing the capacitors to begin to charge. In parallel, a current flows through the copper structure – in one plate, through the bore, and out the other plate. The magnetic switch acts as a high impedance (effectively, a series inductance) during this charging process, allowing only a small leakage current to flow. The EMF produced by this leakage current is sufficient to break down and maintain an ionized plasma. When the switch core saturates, the core becomes essentially zero inductance, allowing the now charged capacitor bank to appear across the inner induction core. The current and magnetic field in the core ramps, generating an EMF which drives current in the plasma through the bore and plasma return holes. The plasma current flowing through the bore of the device generates its own local magnetic field, which acts to compress the plasma current channel. When this field becomes intense enough, a dynamic pinch (Z-pinch) occurs, which collapses the current channel to less than 1 mm diameter in a few tens of nanoseconds – thus compressing and heating the plasma to the point where EUV emission occurs. The formation of the Z-pinch is illustrated in Figure 2.

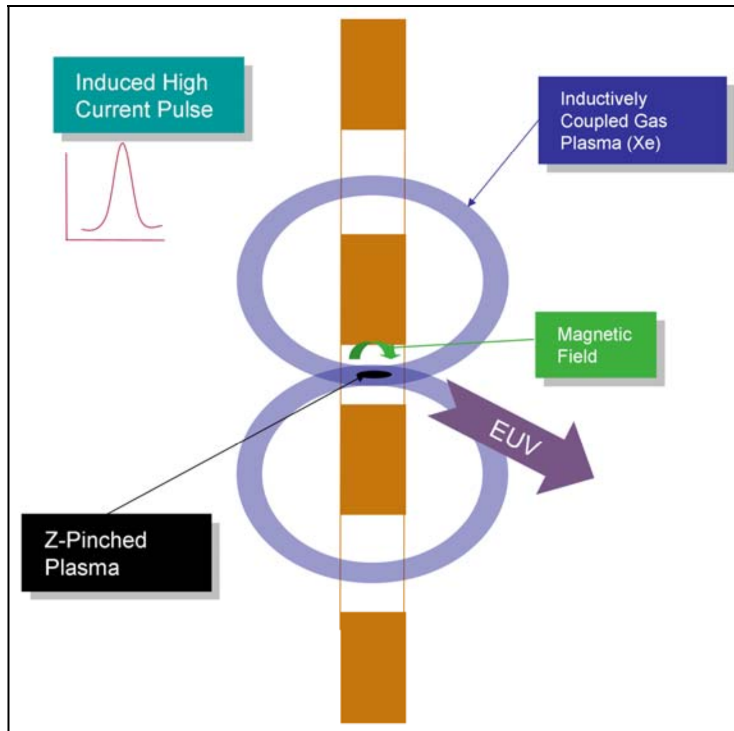

Figure 2. Illustration of the operating principle of the electrodeless Z-pinch light source.

The geometric design of the system deserves mention. The objective, of course, is to ramp the plasma current as quickly as possible. This current is linked to the primary current by the mutual inductance of the inner core. All other sources of stray inductance must be minimized. On the primary side of the circuit, the symmetric parallel plate design accomplishes this goal. On the plasma side, spreading the current among three paths significantly reduces the plasma self-inductance; the large diameter of the return holes (compared to the bore) further reduces the inductance.

Since the plasma current flows in closed loops and does not terminate in metal electrodes, there is no electrode debris produced and no need for frequent replacement of source components. The

magnetic confinement of the plasma loops away from source surfaces results in greater spatial stability and further reduces debris.

The commercial system is relatively simple to operate, with the user controlling source operating parameters through a touch screen interface. It requires minimal routine maintenance (bore replacement every ~billion pulses, or 6 days of 24/7 operation). A photo of a complete system (sans user beamline) is shown in Figure 3.

Figure 3. Photograph of the Energetiq EQ-10 Electrodeless EUV light source.

3. IMPROVED EQ-10 SOURCE

Recently, several key components of the EQ-10 source have been re-designed, with the goals of increasing source radiance, power, and stability, as well as improving system reliability.

3.1 Central bore design

The central bore of the EQ-10 source has been redesigned. This is the component inside which the Z-pinch occurs and that also electrically connects the two source plates, as described in Section 2. The original EQ-10 bore design is illustrated in Figure 4. Here, the electrical connection is made primarily by clamping together adjacent metal surfaces. Also, the inner section of one of the permanent copper plates (the upper plate in Figure 4) is exposed to the pinch plasma, and some eventual wear may occur here.

The new bore design is shown in Figure 5. Now the replaceable component extends through from the face of one plate to the other. All surfaces near the Z-pinch are now removed at the time of a regularly scheduled bore exchange. Moreover, electrical conduction between the plates has been improved by a high current capacity contact insert (as seen on the upper left of the bore in Figure 5). The thickness of copper surrounding the silicon carbide bore insert has increased for improved cooling of the insert. The outer sections of the bore have been tapered to help improve plasma flow and gas fueling to the pinch. Other components of the source plates were reworked to accommodate these changes.

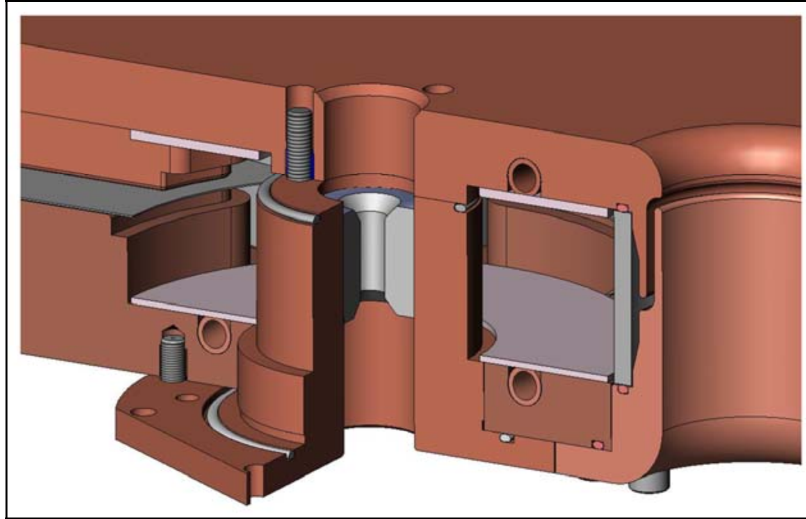

Figure 4. Bore design of original standard EQ-10 source.

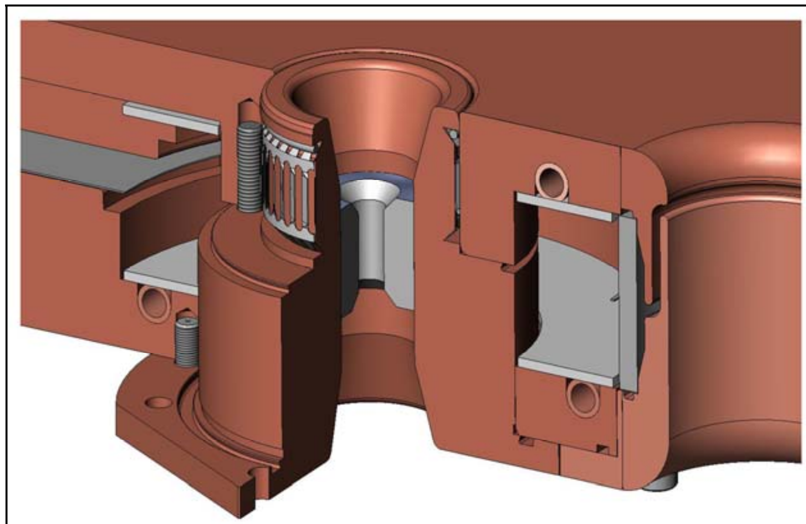

Figure 5. Redesign of bore for new version of EQ-10 source.

3.2 Improved power handling and pulse-to-pulse stability

We have also modified the system to handle more power. This required upgrades both to the modulator (to deliver the power), and to the source itself (to manage the increased thermal loads). Modifications to the source head itself included adding additional internal cooling flow circuits which increased the operating power limits while substantially lowering the operating temperatures of key components. This also reduced the water inlet pressure requirements by half.

The modulator itself was redesigned to accept a higher DC drive voltage. This upgrade had implications for the switch shown at the left in Figure 1(d), since a reflecting pulse from an unmatched load could place up to twice the DC applied voltage across the switch. To ameliorate this condition, a snubber circuit, located at the primary of the step-up transformer in Figure 1(d), was installed to absorb the energy of a reflected pulse.

One can identify, in Figure 1(d), a drive system (DC charging supply, switch, capacitor bank and transformer) coupled to a non-linear transmission line with two sections, which in turn drives a non-linear load. Inconsistent pulse-to-pulse performance can be caused by a reflected pulse from the unmatched, non-linear load coupling back through the transmission line to the charging system. In particular, the charge on the first capacitor bank (which initiates the pulse) will depend on the state of the preceding pulse. Thus, bimodal and even more complex behavior is possible. There is a significant literature on "dynamical" chaos in power delivery systems [8][9][10][11] but what we have here is even more complex, because the plasma itself can also be a source of chaotic behavior [12][13]. It was speculated that the modification of adding a snubber circuit would change the pulse-to-pulse stability behavior; this turned out to be the case as will be shown in Section 4.2.

4. EQ-10 OUTPUT PERFORMANCE

The performance of the standard EQ-10 source has previously been well characterized [14][15]. Here we will review several key aspects that are pertinent for a metrology source, namely stability and brightness. First, it is worthwhile to describe the specific metrology tools used to measure EUV power and size.

4.1 Metrology Tools

Since brightness drives the throughput of any metrology tool, precise, calibrated measurements of source power and size are necessary. Power and imaging measurements allow precise calculation of source brightness. The same tools allow measurement of source stability, both in pulse-to-pulse energy stability and in position and size.

4.1.1 Power

There are various methods of measuring the EUV output power of the source, several examples of which have already been described in past publications [14]. A typical arrangement is shown in Figure 6. The integral components of the power diagnostic are a silicon diode (AXUV100G) and a ±1%BW custom [17] 85° mirror. Two Zirconium foils are used to enable *in situ* foil transmission calibration, and a capacitance manometer is used to monitor the pressure of Xenon in the beamline to correct for gas absorption. In practice, the mounted mirror and photodiode are calibrated at the

SURF facility at NIST, Gaithersburg, MD. The calibration of other power diagnostics are then checked against the NIST calibrated monitor. In addition, we adjust the measurement by taking into account the convolution of the source spectrum and reflectivity of the mirror around 13.5 nm. (This adjustment is on the order of 1% [18]).

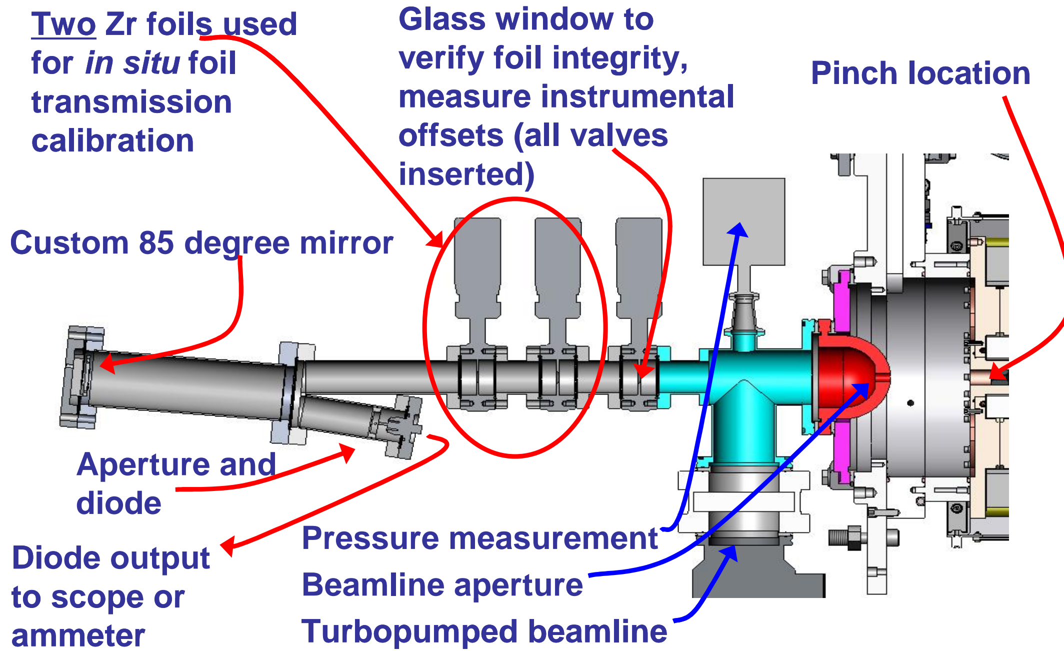

Figure 6. Standard beamline for power metrology using 85° narrow band mirror.

4.1.2 Size/Position

To image the EQ-10 source, we use an x-ray pinhole camera coupled to an Andor DO434-BN CCD. The apparatus has been described in previous publications [14]; some aspects specific to this paper are reviewed here. We obtain an EUV in-band image with the use of a thin Zr foil and an optically flat multilayer mirror (~4% BW) acting as spectral filters. With 1 µm thick Zr foils, the necessary exposure time is typically 0.2 to 1.6 seconds, depending on chosen source operating parameters.

Thus, acquired images are the average of 100's to 1000's of individual pinches. The imaging system can be controlled by computer and is fully automated, so as to capture sequential images over a long time scale of continuous source operation. In order to ensure mechanical stability over these long term tests, special care was taken in mounting the imaging beamline to the source. A rigid framework was constructed that rigidly held the beamline and CCD in place in relation to the source plates, which reduces possible motional degrees of freedom. A sample image and 1-D profile slice can be seen in Figure 7.

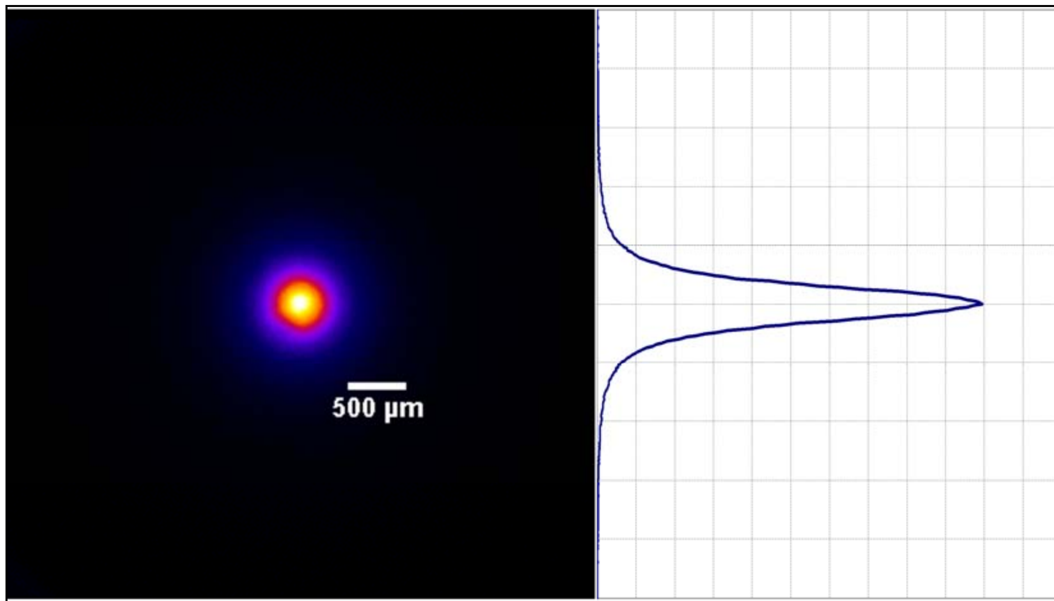

Figure 7. Sample EUV time-integrated pinch image and cross-sectional profile. (False color)

For recent brightness measurements, a 'dual beamline' was developed. The nature of the design of the source does not allow for a wide range of viewing angles. Previously, to obtain the necessary

measurements (power and size) to determine source brightness the diagnostic vacuum beamline had to be switched, requiring turning off the source and venting the vacuum chamber. With two separate beamlines, power and size were measured at different times with different accumulated pulses on the bore (source power and size shift slightly, at a given operating condition, as the bore ages). With the new beamline, we are able to move the imaging 45° mirror into and out of the beamline while under vacuum and with the source operating. Otherwise, the diagnostics are exactly the same as described above. This new beamline allows acquisition of both power and imaging data at the same operating condition nearly simultaneously. This allows for a higher accuracy of the brightness of the EQ-10 source, and for optimizing brightness in near real time. Power, size, and brightness data presented later in this paper were all acquired with this 'dual beamline'.

4.2 Improved pulse-to-pulse stability

Understanding the noise in the source by characterization of pulse-to-pulse stability is critical for metrology tools in order to differentiate defects on the mask from defects in the light pulses. Here, pulse-to-pulse, or dose, stability is measured with the in-band EUV power monitor shown in Figure 6. Data for pulse-to-pulse statistics is acquired using a gated integrator to capture the energy of each individual pulse. Acquisition is triggered at source operating frequency (~ 2 kHz). Typical results for an hour of continuous operation at optimal conditions for stability are a ratio of standard deviation to mean pulse energy $\sigma/\mu < 2\%$ (see, for example, first two values in Table 1), without any data averaging. We note that the source operates open-loop, with no feedback on EUV power.

We compared the pulse-to-pulse reproducibility in detail for several combinations of DC voltage, pulse rate, and xenon pressure. The data was acquired by capturing, integrating and digitizing each

pulse, over a period of many minutes to an hour - typically over one million pulses. Each pulse train was then statistically analyzed. The results for 4 interesting cases are show in Figure 8. Cases A and B are identical plasma conditions, with/without the modulator upgrade, at high chamber pressure; Cases C and D, similarly at low chamber pressure. Table 1 lists the results of several conditions, giving the DC voltage, pulse rate, and chamber pressure in millitorr.

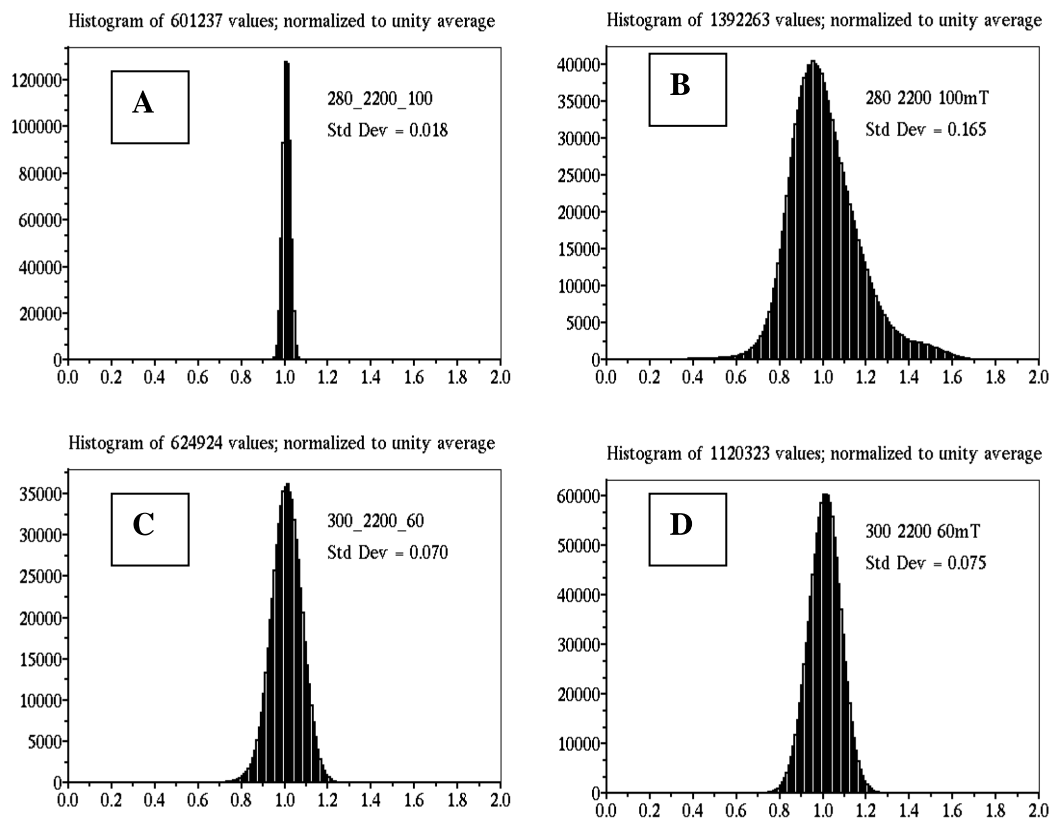

Figure 8. Histograms showing statistics of consecutive pulses, under different conditions. Left side – with upgraded modulator; right – without.

A	B		

Conditions:	Standard Deviation		Ratio
V_Hz_mT	New	Old	Old/New
280_2200_100	0.0179	0.1651	9.20
280_1900_90	0.0190	0.0756	3.97
280_1900_70_2	0.0215	0.0804	3.74
280_1900_110	0.0223	0.1221	5.47
280_2200_80	0.0268	0.1009	3.76
300_2200_80	0.0359	0.0534	1.49
320_1900_100	0.0371	0.0773	2.08
320_1900_80	0.0402	0.0568	1.41
320_1900_60	0.0667	0.0876	1.31
300_2200_60	0.0705	0.0752	1.07

Table 1. C D

Statistics for the four cases displayed as histograms in Figure 8 appear in the top and bottom row. We also display the ratio of standard deviation, (old/new).

It is interesting to observe that, without the modulator modification, the best stability (least standard deviation in the pulse train) occurred at the lowest pressures; the worst, at the highest pressures. With the new modulator, this trend is reversed. Comparing similar conditions, the new modulator has better stability – nine times better at high pressure, but only a marginal improvement at the lowest pressure. The implication is that with the old modulator, the high-pressure instability was caused by the mis-matched load; at low pressure, the load was better matched, and the remaining instability was due to plasma effects. The modifications substantially improved stability due to load mismatch, without (of course) affecting the low-pressure plasma effects. The improved performance observed with the upgraded modulator is significant since the optimum conditions for high brightness are at higher pressure.

4.3 Brightness

Source brightness, or radiance, is determined from a combination of measuring source power into 2π and imaging the source spatial profile. Typical units used by metrology tool makers for source brightness is watts per square millimeter per steradian [$W/mm^2/sr$]. EUV power and size data for the modified EQ-10 are shown in Figure 9 and Figure 11 for a variety of standard source operating conditions. Voltages shown are the DC input voltage to the modulator driving the source, frequency is the pulse repetition rate, and pressure is the Xenon gas pressure inside the source chamber. The input energy per pulse scales as the square of the DC input voltage. For any given combination of pulse rate and input pulse energy, there exist unique pressures such that EUV power is maximized and plasma size is minimized, although these may not occur at the same pressure. The original, pre-modified EQ-10 was limited to sustained input power around 4.5 kW.

The power performance is improved by operating at 7 kW as shown by comparing Figure 9 to Figure 10. Minimum pinch size remains relatively the same (< 400 μm) going to 7 kW as shown in Figure 11. For this data, power and size are measured almost simultaneously, by use of the 'dual beamline' diagnostic described in section 4.1.2.

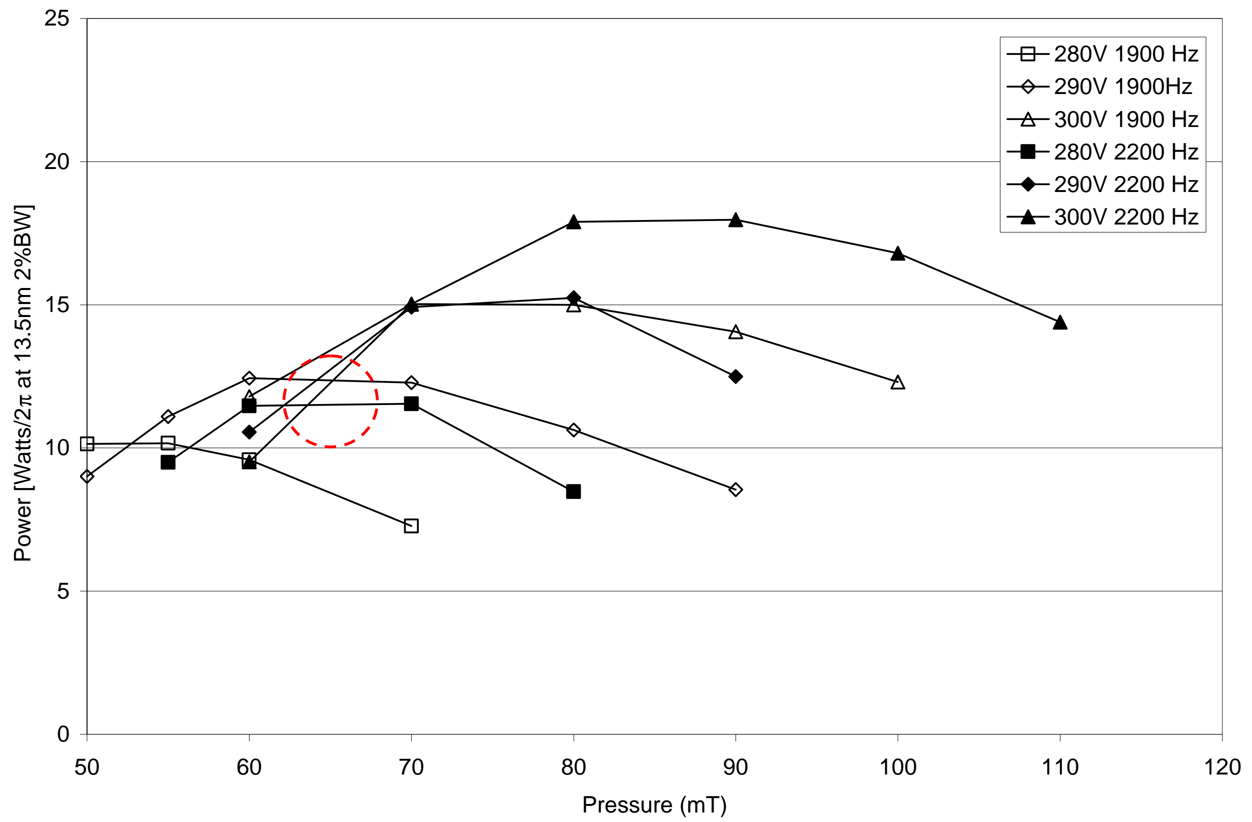

Figure 9. Output power into 2π of the redesigned EQ-10. Dashed circle shows standard operating point for pre-modified source, with ~ 4.5 kW DC input power.

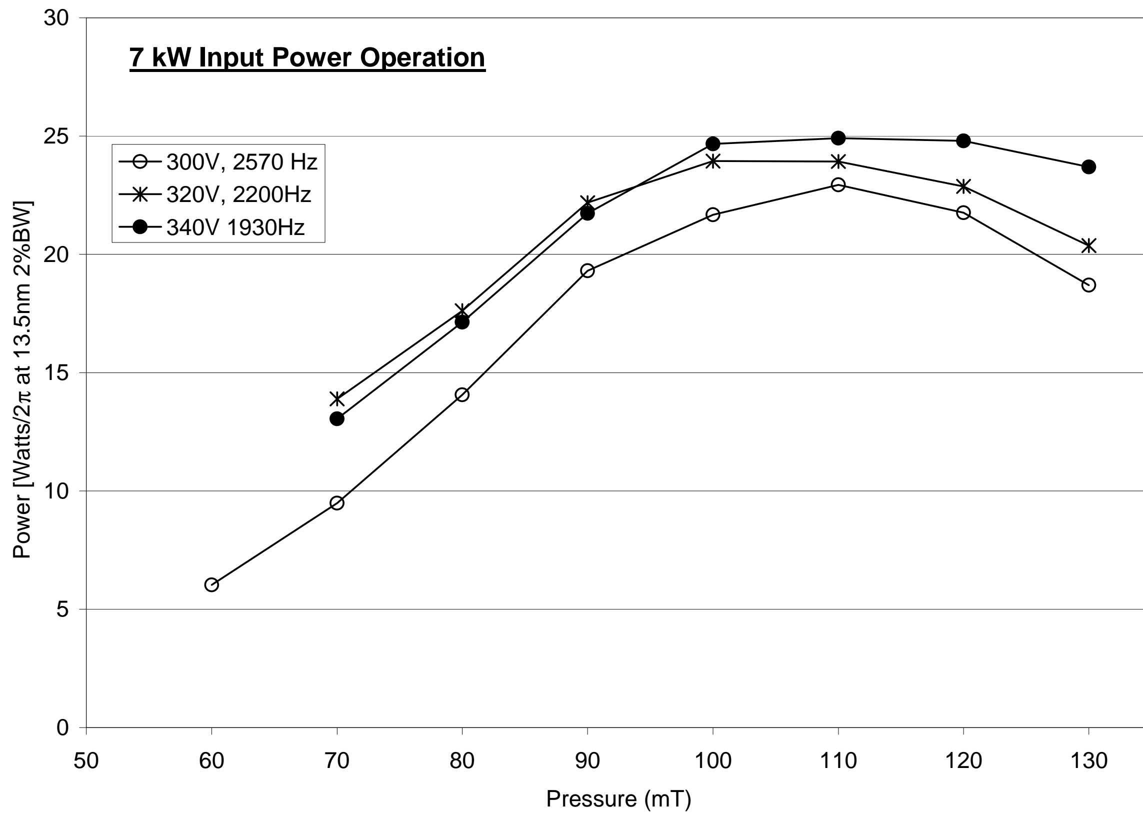

Figure 10. Output EUV power into 2π with 7kW input power of the modified EQ-10 source.

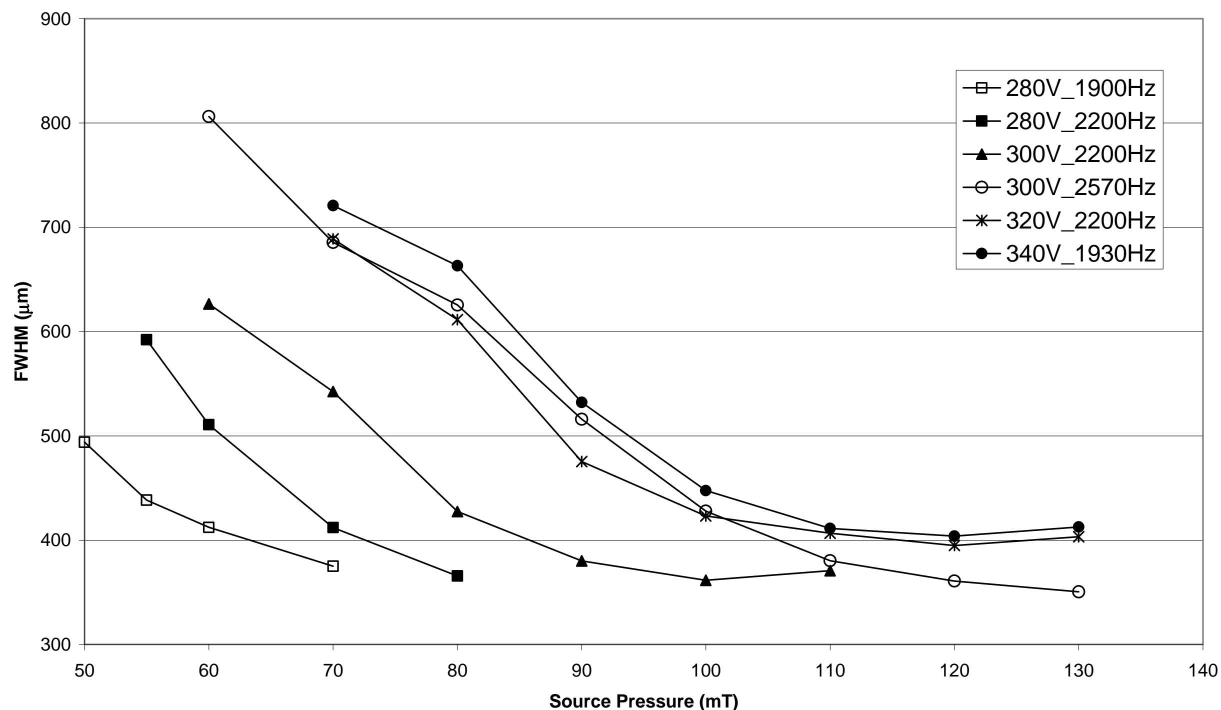

Figure 11. FWHM Source size (EUV ~4% BW) of the redesigned EQ-10 source for various operating parameters, including 7 kW input power.

A 'back-of-the-envelope' method of calculating the source brightness from this data would be to simply take the power into 2π steradians and divide by the area given by the FWHM. However, this overestimates the source brightness as it does not properly account for the distribution of emission both inside and outside the FWHM. The exact plasma intensity profile is critical for estimating peak brightness from integrated power and imaging. For example, consider two different sources that are roughly similar, one with a Gaussian profile and one with a Lorentzian profile, each with identical integrated power and FWHM. Due to the difference in profile, the Lorentzian distribution will have a peak brightness that is only half that of the Gaussian [5]. To estimate the average radiance from

within the FWHM, one could subtract from the total power the fraction of the power that is emanating from outside the FWHM, and use the average power emanating from within for the calculation.

We choose a more explicit representation of source brightness. By angular integration of the entire image as a function of distance from the center of the pinch, the local brightness at specific radius can be calculated. Here brightness is expressed in units of Watts/mm^2/sr, where by 'Watts' is meant the power in 13.5 nm 2% bandwidth. As can be seen in Figure 12, source brightness is improved with the new design, with peak radiance > 8 Watts/mm^2/sr. Note that Figure 12 represents the brightness at a specific radius 'r' from the center of the pinch, and not the average radiance within radius 'r'. Figure 13 shows the peak brightness for several 7 kW operating conditions. There seems to be little dependence on pulse rate or voltage, as long as input power is held constant.

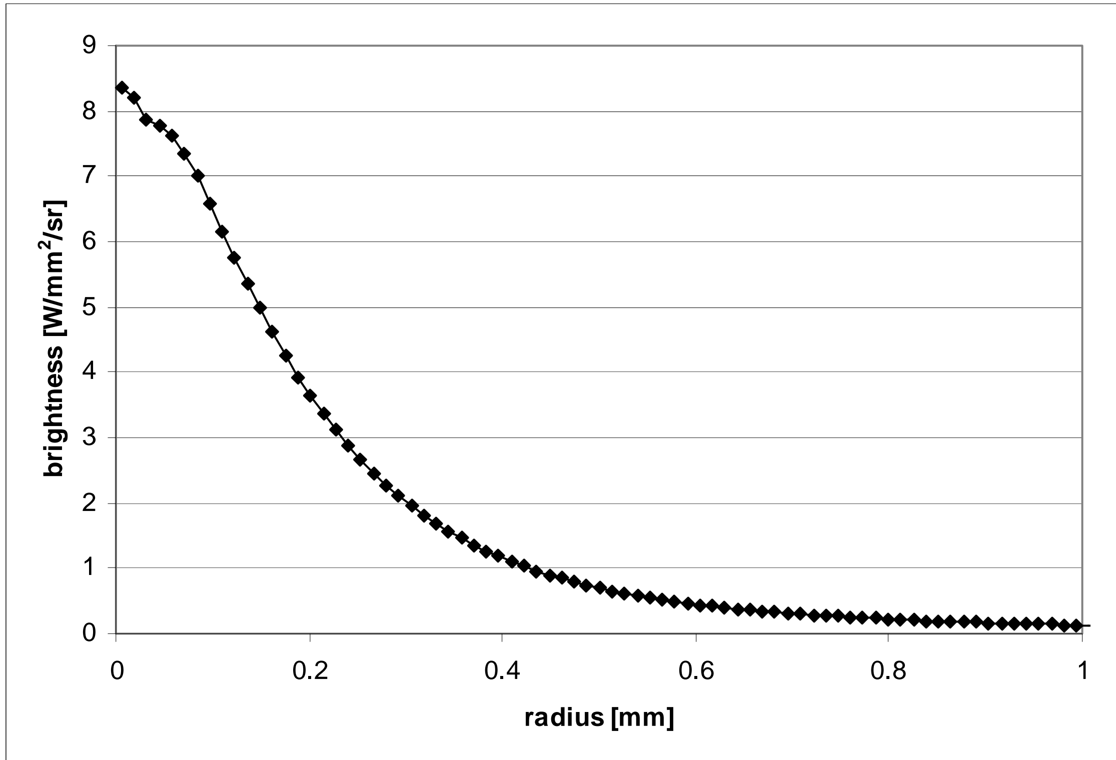

Figure 12. Local brightness at a given distance ‘r’ from the center of the pinch, for the redesigned EQ-10 source, for operating conditions 300V, 2570Hz, and 120mT.

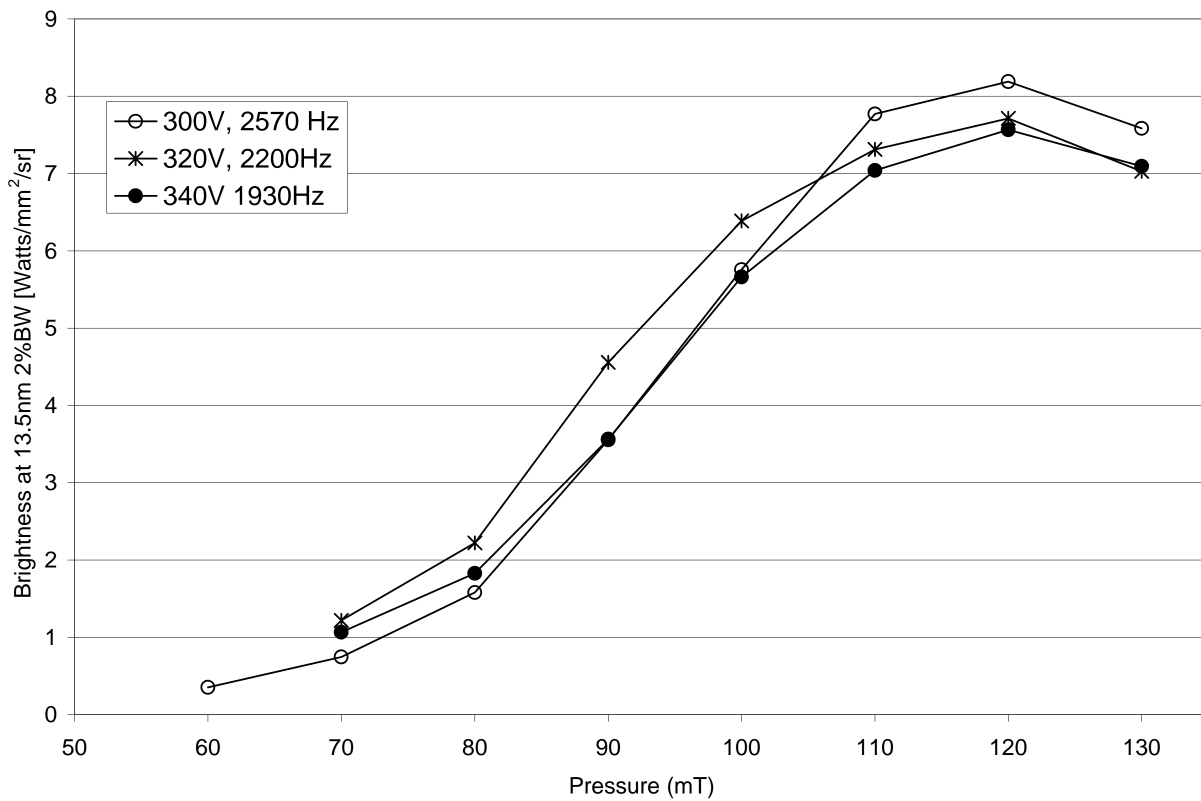

Figure 13. Peak brightness for several 7 kW DC input operating conditions.

4.4 Spatial Stability

Characterized spatial stability, like pulse-to-pulse energy stability, is critical for interpreting metrology signals. Also, spatial instability leads to a reduced average brightness of the source. Figure 14 summarizes the results of a measurement of long-term spatial stability. We imaged the source for 44 hours of continuous operation at 2 kHz pulse rate, capturing an image once every hour (without any feedback to source operating conditions). The size of a pixel on the CCD, referenced to the source plane, was ~13 microns (pinhole imaging was arranged to be ~1:1).

Two statistics were extracted from the data: source size and source position. For size, defined by the FWHM of the pinch, the variation over the total 44 hours was σ = 5 microns with an average FWHM of 400 microns, or about 1% variation. Source position is defined by the centroid of the image. We observed an average deviation from the mean position of ~8 microns, as can be seen in the scatter plot of Figure 14. It should be noted that the observed deviations for both FWHM and position are near the resolution limit of the imaging system. Furthermore, over the course of the 44 hour test, positional deviation was largely effected by the stability of the imaging beamline itself, as the 44 hour test was performed before development of a mechanically rigid beamline. Excellent positional stability is to be expected in this type of source as the current producing the pinch, flowing in the plasma loops, is magnetically confined and makes no contact with source surfaces.

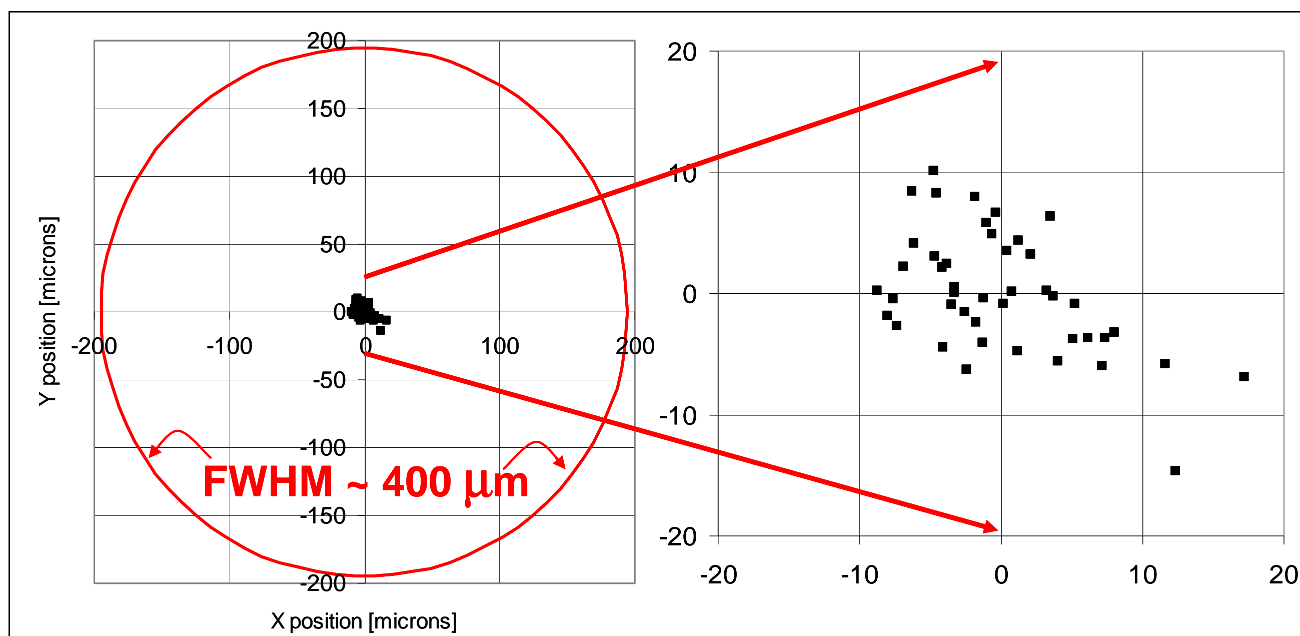

Figure 14. Scatter plot showing source position over 44 hours of continuous operation (~300 million pulses). The source FWHM is shown in left plot at ~400 microns. At

the right is a blow-up showing data points in detail. This measurement is limited by the stability of the mechanical alignment of the diagnostic beamline.

5. SCALING TO HIGHER BRIGHTNESS

To scale the basic electrodeless pinch technology to higher brightness or power, the most obvious route is through frequency. That is, if the emitted EUV per pulse remained constant, then doubling the pulse frequency would double the output. We have explored this approach in some detail. Two independent limits have been found.

First, there is a limit imposed by the pulsed power system. The saturable cores used as magnetic switches (see Figure 1b,d) dissipate energy in the range of a quarter joule per switch. Thus, at our nominal 2 kHz operation frequency, the switch cores dissipate of order 500 watts each. As frequency is raised, cooling these components becomes more and more challenging. We have built a 10 KHz version of the source for use in an optics lifetime testing application [16]; however the engineering tradeoffs required to operate at this frequency (primarily, the electrical energy delivered per pulse had to be reduced) gave an operating point at a lower power and brightness than our standard configuration. In principal, this problem can be overcome with sufficiently clever thermal and electrical engineering – however there seems to be another more restrictive limit to source performance.

The pinch requires fueling with xenon gas at a specific density. As the average input power to the plasma is raised (either through frequency, or by raising the energy per pulse), the ambient xenon gas temperature increases, especially in the location where the pinch forms. The pressure rise in the chamber during plasma initiation is about a factor of two, implying a volume-average temperature increase to about 600 K. However, there are certainly large temperature gradients in the gas, implying that the local temperature near the pinch will be higher. At fixed pressure, increasing the temperature decreases the xenon density near the pinch. As power is raised, at some point this effect prevents adequate xenon from reaching the pinch region. Raising the ambient xenon pressure can compensate only up to a point, as increased gas density between the pinch and the source-to-beamline output port causes more and more absorption of the 13.5 nm light we wish to collect. This effect also occurs if we raise the applied electrical energy per pulse, at fixed frequency. This effect can be seen clearly in Figure 9, where the ambient pressure required to achieve maximum EUV power moves to higher values as input power is increased. Thus, pinch fueling can become a limit to achieving higher power. Novel methods of pinch fueling have been explored [19].

An important point is that requirements for metrology demand higher brightness, not power. The plasma size delivered by the EQ-10 significantly overfills the etendue of a typical metrology design. If plasma size can be reduced at fixed power, brightness will be increased. We have modeled using the EQ10 plasma as a target for a pulsed laser [20]. By optimizing EQ-10 for high plasma density at lower electron temperature, a very spatially and temporally stable, pre-ionized target can be created. By bringing the laser to a 20-50 micron spot we estimate a brightness of order 100 W/mm^2/sr could be achieved, depending on laser power and the ultimate size of the region heated by the laser focus. This approach has the obvious advantage over tin laser-produced plasmas (LPP) [21] of inherent cleanliness – no tin supply or mitigation would be required. While the physics seems

straightforward [22][23][24], a successful proof-of-principal demonstration would be required to motivate the significant engineering effort required to bring this technology to market.

6. CONCLUSIONS

The EQ-10 has proven to be a highly reliable system for EUV metrology. The spatial and temporal stability that is characteristic of the electrode-less design has led to broad acceptance of the device within the EUV community. We have reported here on further development of the EQ-10 to increase power and brightness, and to further improve reliability. The modifications to the source and power delivery systems have roughly doubled the source output from 10W to 20 W, and have increased source brightness to >8 W/mm^2/sr – a level that is adequate for initial actinic aerial imaging mask inspection tools at the 16 nm hp node. Enhancements based on laser heating of the electrodeless Z-pinch could lead to suitable sources for production mask inspection tools.

REFERENCES

[1] D. Smith, S. Horne, M. Besen, P. Blackborow, "Inductively-driven plasma light source." U.S. Patent 7,307,375, issued December, 2007.

[2] Tsuneo Terasawa, Takeshi Yamane, Toshihiko Tanaka, Teruo Iwasaki, Osamu Suga and Toshihisa Tomie, "Development of actinic full-field EUV mask blank inspection tool at MIRAI-Selete", Proc. SPIE 7271, 727122 (2009); doi:10.1117/12.813602

[3] Tsuneo Terasawa, Takeshi Yamane, Toshihiko Tanaka, Osamu Suga, Takashi Kamo and Ichiro Mori, "Actinic phase defect detection and printability analysis for patterned EUVL mask", Proc. SPIE 7636, 763602 (2010); doi:10.1117/12.846678

[4] Takashi Kamo, Tsuneo Terasawa, Takeshi Yamane, Hiroyuki Shigemura, Noriaki Takagi, Tsuyoshi Amano, Kazuo Tawarayama, Mari Nozoe, Toshihiko Tanaka, Osamu Suga and Ichiro Mori, "Evaluation of EUV mask defect using blank inspection, patterned mask inspection, and wafer inspection", Proc. SPIE 7969, 79690J (2011); doi:10.1117/12.879551

[5] Dirk Hellweg, Johannes Ruoff, Alois Herkommer, Joachim Stühler, Thomas Ihl, Heiko Feldmann, Michael Ringel, Ulrich Strößner, Sascha Perlitz and Wolfgang Harnisch, "AIMS EUV: the actinic aerial image review platform for EUV masks", Proc. SPIE 7969, 79690H (2011); doi:10.1117/12.879422

[6] S. Sheshadri, Fundamentals of Plasma Physics, American Elsevier Publishing Company, New York, 1973.

[7] Keith A. Munson, Uri Shumlak and Brian A. Nelson, "Extreme ultraviolet light production from a ZaP flow z-pinch xenon plasma", J. Micro/Nanolith. MEMS MOEMS 7, 013003 (Mar 28, 2008); doi:10.1117/1.2898515

[8] J. R. Wood, "Chaos: a real phenomenon in power electronics," pp. 115-124. [Online]. Available: http://dx.doi.org/10.1109/APEC.1989.36959

[9] A. A. Balyakin and N. M. Ryskin, "Chaotic Oscillations in a Nonlinear Lumped-Parameter Transmission Line," Radiophysics and Quantum Electronics, vol. 44, no. 8, pp. 637-644, August 2001. [Online]. Available: http://dx.doi.org/10.1023/A:1012529706961

[10] J. H. B. Deane, "Modeling the dynamics of nonlinear inductor circuits," IEEE Transactions on Magnetics, vol. 30, no. 5, pp. 2795-2801, Sept 1994. [Online]. Available: http://dx.doi.org/10.1109/20.312521

[11] G. K. Vinogradov, "Transmission line balanced inductive plasma sources," Plasma Sources Science and Technology, vol. 9, no. 3, pp. 400+, August 2000. [Online]. Available: http://dx.doi.org/10.1088/0963-0252/9/3/318

[12] T. Braun, J. A. Lisboa, R. E. Francke, and J. A. C. Gallas, "Observation of deterministic chaos in electrical discharges in gases," Physical Review Letters, vol. 59, no. 6, pp. 613-616, Aug 1987. [Online]. Available: http://dx.doi.org/10.1103/PhysRevLett.59.613

[13] P. Y. Cheung and A. Y. Wong, "Chaotic behavior and period doubling in plasmas," Physical Review Letters, vol. 59, no. 5, pp. 551-554, Aug 1987. [Online]. Available: http://dx.doi.org/10.1103/PhysRevLett.59.551

[14] S. F. Horne, M. M. Besen, D. K. Smith, P. A. Blackborow, and R. D'Agostino, "Application of a high-brightness electrodeless Z-pinch EUV source for metrology, inspection, and resist development," Proc. SPIE, 6151, 201-210 (2006).

[15] P. A. Blackborow, M. J. Partlow, S. F. Horne, M. M. Besen, D. K. Smith, and D. S. Gustafson, "EUV Source Development at Energetiq," Proc. SPIE, 6921(1), 692121 (2008).

[16] Stephen F. Horne, Fred M. Niell, Matthew J. Partlow, Matthew M. Besen, Donald K. Smith, Paul A. Blackborow, and Deborah Gustafson, "Development of a high-pulse-rate EUV source," Proc. SPIE, 7271, 72713A (2009)

[17] E. Gullickson. Personal communication

[18] S. Horne, M. Partlow, M. Besen, D. Smith, P. Blackborow, and D. Gustafson, “EUV Source Development at Energetiq Technology,” in International Symposium on Extreme Ultraviolet Lithography, Sapporo, Japan, Sematech, 2007. Proceedings available from SEMATECH, Austin, TX.

[19] D. Smith, S. Horne, M. Besen, P. Blackborow, R. Collins "Inductively-driven plasma light source." U.S. Patent 7,948,185, issued May, 2011

[20] Stephen F. Horne, Matthew M. Besen, Matthew J. Partlow, Donald K. Smith, Paul A. Blackborow, Deborah S. Gustafson, “High brightness Electrodeless Z-Pinch™ EUV Source for Mask Inspection Tools,” submitted to International Symposium on Extreme Ultraviolet Lithography, Miami, Florida, USA, SEMATECH, October 2011.

[21] V. Bakshi, EUV Sources for Lithography (SPIE Press Monograph Vol. PM149), SPIE-International Society for Optical Engineering, 2006.

[22] S.Wieneke, S. Bruckner, and W. Viol, “Laser assisted heating of extreme ultraviolet-emitting z-pinch plasmas,” Physics of Plasmas, vol. 15, no. 12, pp. 122 508+, 2008.

[23] J. E. Tucker and R. M. Gilgenbach, “Soft x-ray emission from a co2 laser-heated z-pinch plasma,” Plasma Chemistry and Plasma Processing, vol. 7, no. 3, pp. 365–376, September 1987.

[24] E. S. Wyndham, J. D. Kilkenny, H. H. Chuaqui, and A. K. L. Dymoke-Bradshaw, “An observation of a high heat flux in a laser-heated plasma,” Journal of Physics D: Applied Physics, vol. 15, no. 9, pp. 1683–1688, 1982.

[25] Stephen F. Horne, Deborah Gustafson, Matthew J. Partlow, Matthew M. Besen, Donald K. Smith and Paul A. Blackborow, "Improvements in the EQ-10 electrodeless Z-pinch EUV source for metrology applications", Proc. SPIE 7969, 79692Z (2011); doi:10.1117/12.880794

Biographies to be submitted on revision.

Disclosure: This article contains new data (Figure 9, Figure 10, Figure 11, Figure 12, and Figure 13) as well as data previously published in [15] and [25].